Progress In Electromagnetics Research C, Vol. 119, 49–63, 2022

The Design and Implementation of an RF Energy Harvesting System Using Dynamic Pi-Matching, Enabling Low-Power Device Activation and Energy Storage

B. V. S. Suwan[1], W. W. G. Vidula[2], W. K. I. L. Wanniarachchi[1], C. H. Manathunga[1], and S. Jayawardhana[1, *]

Abstract—Radio-frequency electromagnetic waves can be harnessed to produce an alternative source of energy to replace batteries in many low-power device applications. An efficient radio frequency energy harvesting circuit was designed and constructed using a dynamic Pi-matching network in order to convert frequency-modulated electromagnetic waves in the range of 88–108 MHz to direct current through a 3-step process. The circuit consists of a 50 Ω copper plate dipole antenna, a Pi impedance matching network, and a five-stage voltage doubler circuit. These three modules are connected through SubMiniature version A (SMA) connectors for convenient assembly. The dynamic Pi matching technique for RF energy harvesting is theoretically explained and simulated in the Advance Design System software environment. The experimental values obtained in this proposed work are in good agreement with the simulations. The harvesting system is capable of producing up to 14.3 V direct current voltage across a 100 kΩ load in field tests carried out at a displacement of 760 m from a transmission tower. At 6.7 km from the tower, a DC value of 61.5 mV was still obtainable at the ground level. The direct-current power that was generated through the energy harvesting was applied for the demonstration of three tasks with satisfactory results: illuminating a light-emitting diode, energy storage in a Panasonic VL2020 rechargeable battery, and activation of a TMP20AIDCKT temperature sensor in an urban area which enabled low power device activation and energy storage.

1. INTRODUCTION

Due to technological advancements in communication and the need for extending its outreach across geographical locations, radio frequency (RF) transmitting stations are on the increase. As a result, the level of RF radiation present in the environment is also on the increase. This RF radiation provides a source of "free energy" that can be used to drive low-power electronic devices. This wasted electromagnetic energy can be utilized by converting it into direct-current (DC) energy. The antenna captures this RF energy as alternating electric waves according to a variation in the received electric fields that pass through the antenna. This induced RF energy can be converted into DC energy by sending through a voltage doubler circuitry. In recent years, there has been much interest directed into this area of research, focusing mainly on energy harvesting techniques [1, 2]. The fact that such harvested energy can be considered as green energy and the possibility of storing the harvested energy utilizing an energy storage device such as a battery for later use are two main factors that make the technique attractive.

Received 18 December 2021, Accepted 23 February 2022, Scheduled 9 March 2022

* Corresponding author: Sasani Jayawardhana (sasanijay@sci.sjp.ac.lk).

[1] Department of Physics, University of Sri Jayewardenepura, Gangodawila, Nugegoda, Sri Lanka. [2] Department of Electrical and Computer Engineering, The Open University of Sri Lanka, Sri Lanka.

GSM frequency bands which are designated for the use of GSM mobile phones and devices span the range between 380 MHz and 1900 MHz, with different regions and networks covering sub-ranges derived from the above. Numerous investigators have carried out experiments for RF power harvesting in this range and report output levels varying from 0.05 to 2.9 V at distances varying anywhere between 4 m and 50 m while employing various methodologies for the implementation of the technique [3–8]. It is not straightforward to compare all of these attempts as the output measurement techniques and parameters are not consistent across these experiments. Nevertheless, these experiments could not achieve a significant amount of radio frequency power with significant displacement from the transmission tower.

RF power harvesting has also been investigated in the Industrial, Scientific and Medical (ISM) radio frequency band. The feasibility of various antenna designs such as microstrip patch antennas, rectennas, single element patch antenna, and antenna arrays have been demonstrated by activating sensor nodes or through RF-DC conversion [9–11]. All of these investigations report energy harvesting distances in the centimeter scale which is not a feasible solution. Further, the amount of radio-frequency power achieved is insignificant for a practical application.

In contrast to the single-band power harvesting systems that were described above, there have been several attempts at designing multi-band RF power harvesting systems, which are capable of harvesting RF power from different frequency bands simultaneously [12–14]. Nonetheless, these experiments have fallen short of reaching transduction power on the mW level due to the low power levels of those bands.

An RF power harvesting system designed by employing a small loop antenna and a folded dipole as receiving antennas is reported in the research literature. The specialty of the small loop antenna is that it has a low perimeter compared with the wavelength; therefore, the antenna has been designed to be small like a coin. At 300 MHz, the authors have achieved 0.8 V open-circuit voltage at a distance of 2 m from a 100 mW RF transmitted base station [15].

Complementary metal-oxide-semiconductor (CMOS) technology has also been utilized in the transductor module for increasing the efficiency of RF-DC conversion but has failed to outperform Schottky diode-based transductors due to very low forward voltage drop of Schottky diode [16–19].

Overall, investigators have been incapable of harvesting a significant amount of RF power (in milliwatts level) at a practically viable distance from the transmitting tower. Therefore, there is a necessity for a longer-distance RF energy harvesting system to store RF energy and activate low power devices. In this article, a novel radio-frequency energy harvesting system is presented. The system is implemented with the aim of energizing low-power devices. Further, a system is designed for storing the harvested power for later use. The system is demonstrated to generate 14.3 V across the 100 kΩ load at a 760 m displacement from the transmission tower. Special features of the system are a plate dipole antenna, the dynamic Pi impedance matching technique for RF energy harvesting purposes, an energy storage system, and an operating frequency band. The novelty aspects of each of these will be discussed in the following sections.

2. THE VHF RECEPTION ANTENNA

The reception antenna is discussed under three main categories: i. The VHF reception antenna design and optimization, ii. The antenna methodology, iii. Investigation of the performance of the antenna in the field.

2.1. The Antenna Design and Optimization

The copper plate dipole antenna was designed for capturing very high frequency (VHF) electromagnetic waves from the environment. Copper was the material of choice for the dipole antenna owing to its superior electrical conductivity. The proposed antenna impedance is approximately equated to 50 Ω with low reactance within the 88–108 MHz band. This particular frequency band is used worldwide for broadcasting purposes. The two poles of the antenna were reserved by a 0.55 mm thick copper plate (Agrawal metal works, India). The two copper plates were soldered on a prototype printed circuit board (PCB) using a 60%/40% Tin-Lead compound. The two poles were coupled to an SMA connector through ceramic capacitors for capturing electromagnetic wave energy that is delivered to the conversion module. The antenna fabrication topology is shown in Figure 1(a). The length of a plate (L), the width

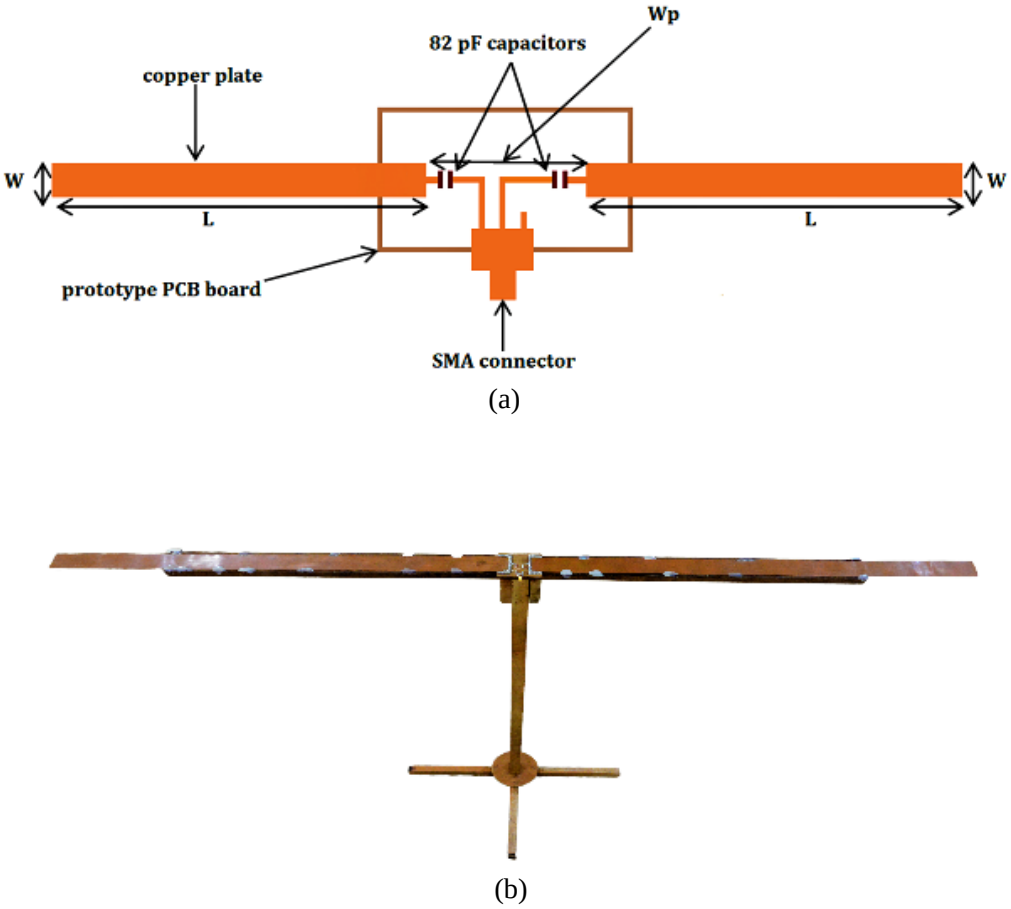

Figure 1. The copper plate dipole antenna showing (a) schematic configuration and (b) actual image.

of a plate (W), and the space between two copper plates (W_p) were optimized to approximate antenna resistance to 50 Ω in the 88–108 MHz frequency range. Two 82 pF ceramic capacitors were coupled in series to each copperplate to minimize antenna reactance. As shown in Figure 1(b) the copper plate dipole was placed on a wood stand. The values for L, W, and W_P were chosen as 75 cm, 4 cm, and 3 cm to obtain a good reflection coefficient value.

2.2. The Antenna Methodology

The antenna reflection coefficient characteristics were measured and optimized through a vector network analyzer (VNA). The antenna performance can be evaluated by investigating the reflection coefficient variation of an antenna [20, 21]. The logarithmically projected scale of reflection coefficient can be represented by the term S_{11} given in Equation (1) [22, 23].

$$S_{11} = 10 \log_{10} \left(\frac{P_r}{P_{in}} \right) \text{ dB} \tag{1}$$

where P_{in} is the power incident on the antenna under test (AUT), P_r the power reflected back to the source, and S_{11} a scattering parameter where the negative value of S_{11} is called the return loss [24]. According to Equation (1), the more negative the value of S_{11} is, the higher the reduction is in reflected power from the antenna. In other words, with more negative value of S_{11} for an antenna, the impedance mismatch is reduced so that the impedance of the antenna can approach the targeted value. The reflection coefficient variation of the designed antenna is shown in Figure 2(a), and the corresponding impedance variation in the Smith chart is shown in Figure 2(b).

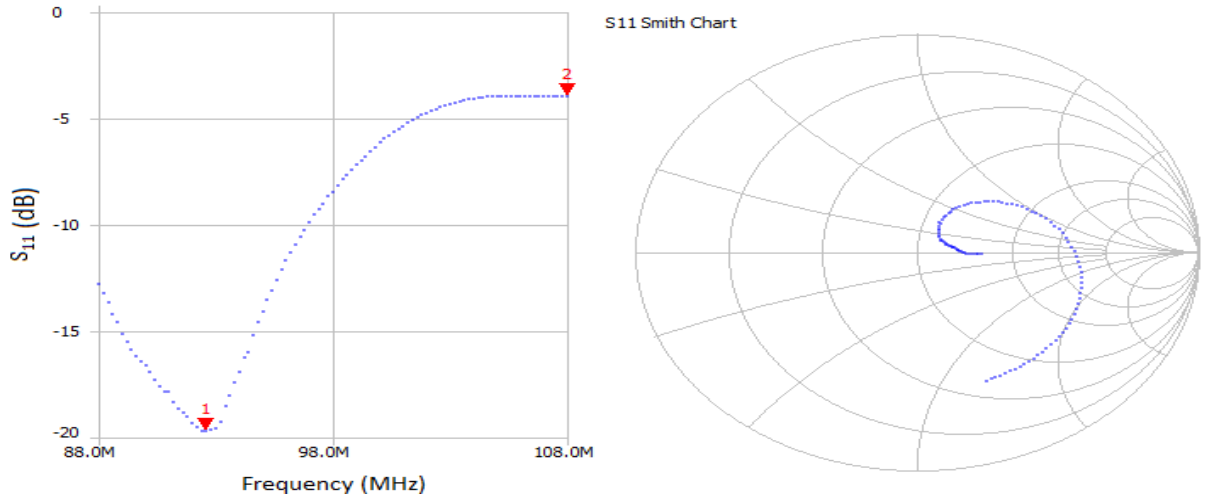

(a) (b)

Figure 2. Test results of the designed antenna with (a) the reflection coefficient variation and (b) the impedance variation given by the Smith Chart.

As evident in Figure 2, the reflection coefficient of the antenna is a negative value throughout the 88–108 MHz band. The lowest value −19.7 dB is reached at 92.6 MHz whereas the highest value −3.9 dB is found at 108 MHz where it has leveled off. Therefore, the reflection coefficient is found to vary between −19.7 dB and −3.9 dB through the entire band. This is a superior performance compared to that of the antenna reported by Khalid et al. [25]. Several other experiments that have attempted to make low deamination antennas such as FM chip antennas have not reported favorable reflection coefficient values through this band [26, 27].

2.3. The Antenna Performance

The constructed 50 Ω copper plate dipole antenna was used to capture radio frequency signals from the environment. A 2 m length of Standard RG-58C/U 50 Ω antenna cable was used to connect the antenna feed point to the spectrum analyzer input for the investigation of the antenna performance. According to the VNA reading, the loss in the antenna cable was 0.6 dB which is negligible. The performance of the antenna was investigated at two locations as described below.

Location 1: At this location, the investigation was carried out at the ground level with 6.7 km displacement from the nearest 88–108 MHz FM signals transmission tower. To investigate the capturing of radio signals by the antenna, the entire bandwidth (100 kHz–500 MHz) of the spectrum analyzer was used. The result spectrum form is shown in Figure 3. It was shown that a high amount of RF power is captured from 88–108 MHz range radio signals due to the antenna's impedance matching with the input impedance of the spectrum analyzer which is 50 Ω. At that range, the antenna shows a more negative reflection coefficient variation. To ascertain the individual radio stations, the bandwidth of the spectrum analyzer was adjusted to 88–108 MHz range. This resulted in 49 peaks on the power spectrum. The resulting power spectrum form is shown in Figure 3, and the corresponding spectrum analyzer readings are shown in Table 1.

Location 2: The 50 Ω copper plate dipole antenna was employed at a 32 m height from ground level with a 760 m displacement from the nearest transmission tower. The antenna captured 58 radio channels at this location. The resulting spectrum form is shown in Figure 4, and the corresponding spectrum analyzer readings are presented in Table 2.

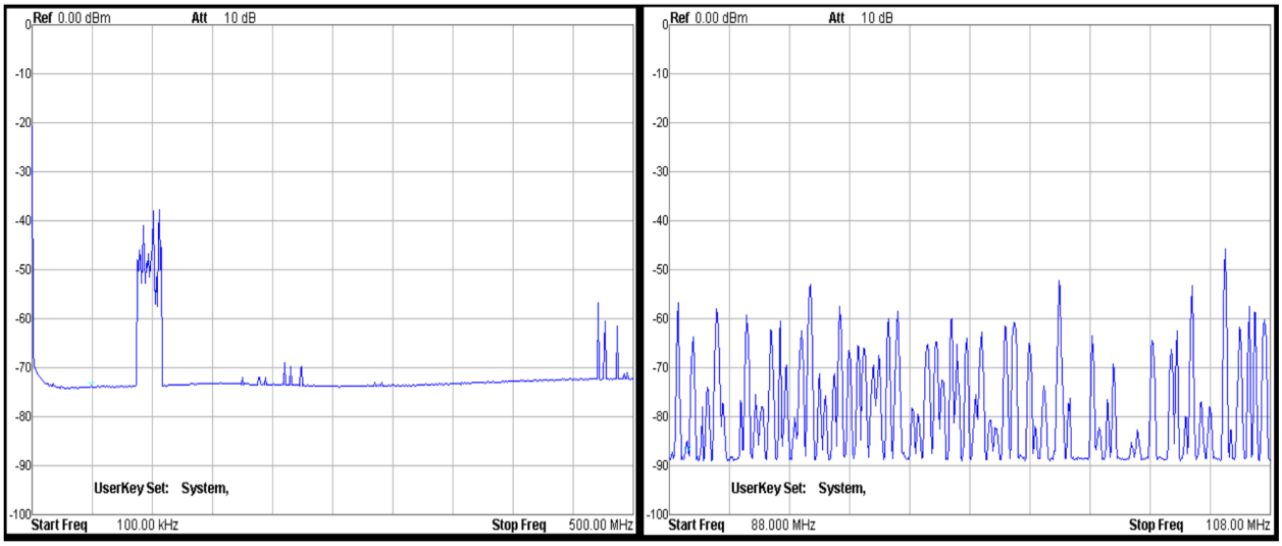

(a) (b)

Figure 3. Antenna field test spectrum form at location 1 when spectrum analyzer bandwidth (a) 100 kHz–500 MHz range, (b) 88 MHz–108 MHz range. The x-axis represents the frequency in MHz while the y-axis represents power in dBm.

Table 1. Field test readings of the antenna at location 1.

Captured radio station frequency (MHz)	Received Signal Strength (dBm)	Captured radio station frequency (MHz)	Received Signal Strength (dBm)	Captured radio station frequency (MHz)	Received Signal Strength (dBm)	Captured radio station frequency (MHz)	Received Signal Strength (dBm)
88.26	−59.41	93.20	−74.45	98.36	−63.23	104.73	−68.35
88.76	−62.37	93.46	−68.71	98.56	−81.69	104.86	−71.20
89.26	−70.63	93.66	−55.10	99.16	−59.78	105.36	−55.72
89.56	−60.01	93.96	−67.96	99.50	−59.53	105.66	−73.82
90.40	−70.35	94.30	−66.81	99.96	−65.47	105.96	−71.37
90.60	−55.72	94.50	−67.88	100.50	−72.52	106.50	−45.92
91.06	−76.54	94.96	−66.99	101.00	−53.45	107.00	−64.63
91.40	−61.60	95.26	−63.65	101.30	−62.59	107.26	−54.48
91.70	−61.97	95.60	−58.4	102.10	−64.13	107.50	−64.05
91.86	−74.24	96.06	−70.95	102.60	−77.30	107.76	−59.58
92.40	−61.27	96.56	−63.11	102.76	−66.98		
92.66	−50.12	96.90	−63.85	103.60	−77.57		
93.00	−70.16	97.13	−71.20	104.06	−63.00		

3. THE IMPEDANCE MATCHING NETWORK

This section describes a dynamic Pi impedance matching technique for the RF power harvesting system under two main categories: i. methodology of the Pi matching technique, ii. performance of Pi matching technique verified by simulation and implementation results.

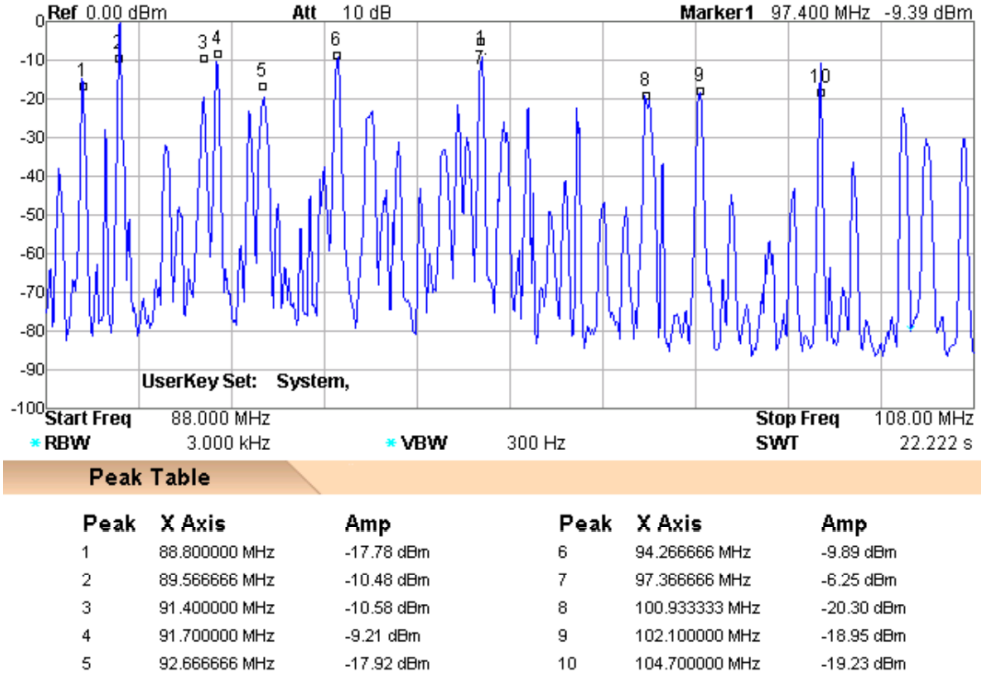

Figure 4. Antenna field test spectrum form at location 2. The x-axis represents the frequency in MHz while the y-axis represents power in dBm.

Table 2. Field test readings of the antenna at location 2.

Captured radio station frequency (MHz)	Received Signal Strength (dBm)	Captured radio station frequency (MHz)	Received Signal Strength (dBm)	Captured radio station frequency (MHz)	Received Signal Strength (dBm)	Captured radio station frequency (MHz)	Received Signal Strength (dBm)
88.06	−68.33	92.66	−17.92	97.36	−7.71	102.76	−44.87
88.23	−42.69	92.96	−46.33	97.90	−29.86	103.00	−77.36
88.80	−17.78	93.16	−64.12	98.03	−45.20	103.60	−55.51
89.06	−65.28	93.43	−61.56	98.31	−55.15	104.41	−42.85
89.30	−33.31	93.66	−55.08	98.36	−25.21	104.70	−19.23
89.56	−10.48	94.00	−37.78	98.56	−56.94	105.20	−64.36
90.36	−67.50	94.26	−9.89	98.90	−48.33	105.40	−36.06
90.60	−28.69	94.46	−57.87	99.20	−39.26	105.70	−75.70
90.86	−48.22	95.00	−21.10	99.43	−24.38	106.46	−20.00
91.06	−61.10	95.26	−42.07	100.03	−46.14	106.80	−51.06
91.40	−10.58	95.63	−35.08	100.50	−48.76	107.00	−26.00
91.70	−9.21	96.10	−43.89	100.93	−20.30	107.16	−56.32
91.96	−64.00	96.53	−30.35	101.26	−41.75	107.80	−25.97
92.10	−54.45	96.90	−28.23	102.10	−18.95		
92.33	−25.90	97.00	−31.61	102.56	−62.50		

3.1. Methodology of Pi Matching Technique

For the purpose of transferring the captured RF power to the voltage doubler circuitry, the impedance matching network is one of the main stages of RF power harvesting systems. Figure 5 shows a low-pass configuration of a Pi matching network between a source and a load.

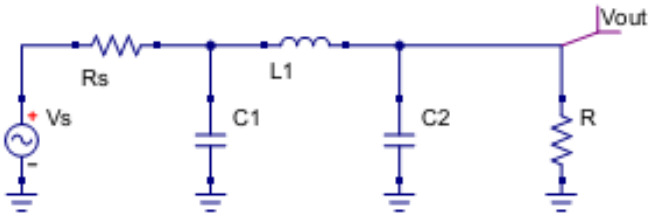

Figure 5. The Pi impedance matching network between a load and a source.

The output voltage across the load R can be represented by the following equation

$$V_{out} = \frac{R}{\sqrt{\left[R + R_s - X_L\left(Q + Q'\right)\right]^2 + \left[QR_s + Q'R - X_L\left(QQ' - 1\right)\right]^2}} \times V_s \tag{2}$$

where $Q' = R_s\omega C_1$; V_{out} refers to the voltage across the R load; X_L is the reactance of inductor L_1; and R_s is the resistance of the source.

As shown in Figure 6, the low-pass configuration of the Pi matching network can be shown as two back-to-back L matching networks [28]. The resistor R_V is a virtual resistor which is defined by the desired loaded quality factor of the Pi matching circuitry [28]. The Q is the loaded quality factor of the L matching network on the load side of the Pi network.

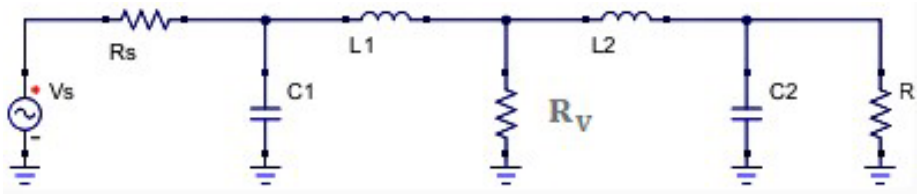

Figure 6. The Pi matching network as a two back-to-back L matching network.

Equation (2) indicates that the output voltage across the load can be increased by reducing the Q value at a considered frequency. Therefore, power transfer from source to load can be maximized by reducing the value of Q.

3.2. Performance of the Pi Matching Technique

The proposed Pi matching technique was simulated in the Advanced Design System (ADS, Keysight technology) environment. As shown in Figure 7, in order to investigate the scattering parameter S_{11},

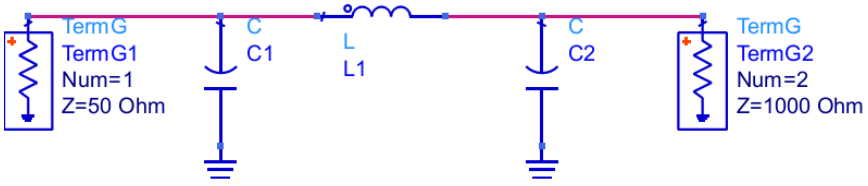

Figure 7. The Pi matching network between 50 Ω and 1000 Ω port impedance terminations for S-parameters.

Table 3. Evaluated lumped components values for each Q value.

Q Value	Value of L_1 (nH)	Value of C_1 (pF)	Value of C_2 (pF)
4.4	361.67	4.36	7.15
5.0	346.53	17.79	8.12
10.0	193.15	65.37	16.24
15.0	130.85	104.24	24.36
20.0	98.68	141.77	32.48

the simulation process was done between 50 Ω source and 1000 Ω load with varying Q values. Table 3 presents the evaluated values of lumped components for each Pi matching network.

The simulated scattering parameter variation graph is shown in Figure 8(a). The red, blue, pink, green, and purple curves represent Pi matching networks with Q values of 4.4, 5.0, 10.0, 15.0, and 20.0, respectively. As shown in Figure 8, all circuits were designed to resonate at the central frequency of the band which is 98 MHz. Markers m_1 and m_3 on the curve with a Q value of 5 correspond to 94 MHz and 102 MHz points while markers m_2 and m_4 are on the curve with a Q value of 15 and correspond to 94 MHz and 102 MHz points. The S_{11} values at 94 MHz of points m_1 and m_2 are −14.263 dB and −4.947 dB, respectively, while for the points m_3 and m_4 at 102 MHz they are −13.777 dB and −4.286 dB. Therefore, when considering these four points, m_1 has a lower S_{11} value than m_2 at 94 MHz, and m_3 also has a lower S_{11} value than m_4 at 102 MHz. Furthermore, the point m_1 is on a low Q value curve compared with point m_2, and point m_3 is also on a low Q value curve compared with m_4. Therefore, a low Q value for a Pi matching network is more suitable for RF energy harvesting systems due to their comparatively lower S_{11} values through the band.

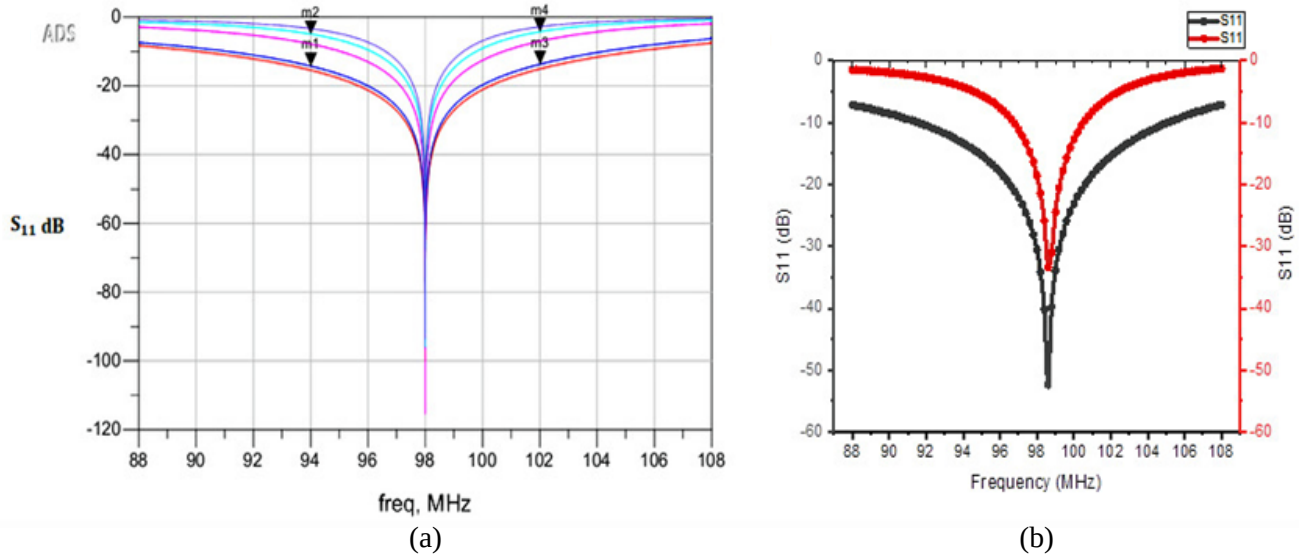

Figure 8. Simulation results of Pi matching technique for S_{11} (dB) versus frequency (MHz) according to (a) simulation and (b) experiment.

The experimental measurements of the scattering parameter variation, when Q is 5 (black), and Q is 15 (red), are shown in Figure 8(b). According to the graph, both $Q5$ and 15 circuits resonate at 98.6 MHz. The low value loaded quality-factor graph ($Q = 5$ graph) shows much greater S_{11} variation through the entire band which is agreement with the simulations.

For characterizing the captured RF power from the harvesting system, a 100 kΩ resistor was connected to the output of the RF-DC conversion module. The input impedance of the 100 kΩ load

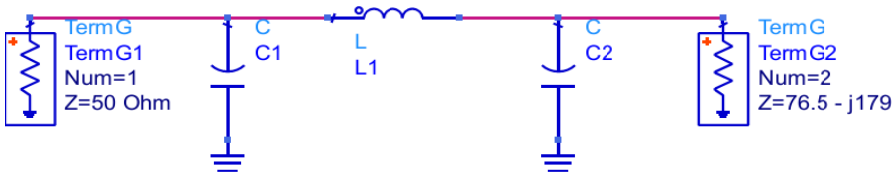

Figure 9. The Pi matching network between $50\,\Omega$ and $76.5 - j179\,\Omega$ port impedance terminations for S-parameters.

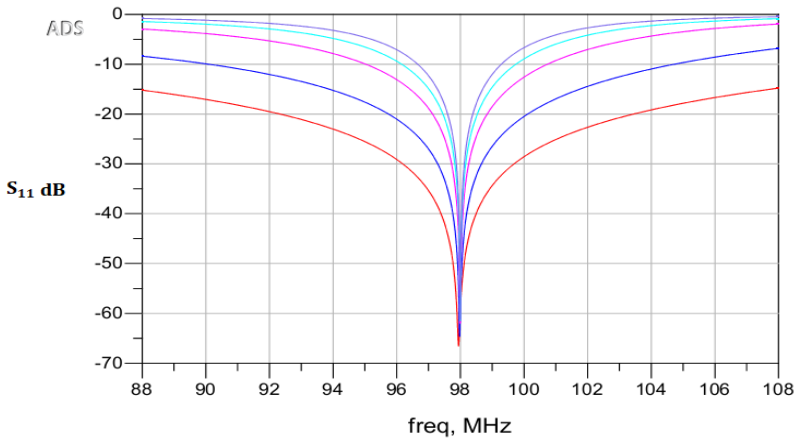

Figure 10. Simulation results of each Pi matching circuitry for S_{11} (dB) versus frequency (MHz).

connected to the RF-DC conversion module was measured as $76.5 - j179\,\Omega$ by the vector network analyzer as shown in Figure 9.

For the design and optimization purpose of the Pi matching circuit between the $50\,\Omega$ antenna and $76.5 - j179\,\Omega$ input impedance, computer simulation was carried out for different Q values for Pi matching circuits. The results are shown in Figure 10. The red, blue, pink, green, and purple curves represent the Pi matching networks with Q values of 3.0, 5.0, 10.0, 15.0, and 20.0. The lowest Q value circuitry was chosen for the harvesting system due to the lowest S_{11} variation through the band. Table 4 presents the calculated values of lumped components for each circuit.

Table 4. Calculated lumped components values for each Pi matching network.

Q Value	Value of L_1 (nH)	Value of C_1 (pF)	Value of C_2 (pF)
3.0	248.77	2.82	2.15
5.0	194.44	41.33	8.70
10.0	103.97	98.39	25.06
15.0	70.13	151.55	41.42
20.0	52.81	203.88	57.78

As shown in Figure 11, the low Q value of Pi matching networks was designed for each input impedance of the RF-DC conversion module. Table 5 presents the lumped components values for each circuit.

As shown in Figure 12, Panasonic VL2020 battery and energizing low power devices, such as TMP20 temperature sensor and a light-emitting diode (LED), were connected to the output of the RF-DC conversion module. Each circuitry was connected to the vector network analyzer to measure the input impedance.

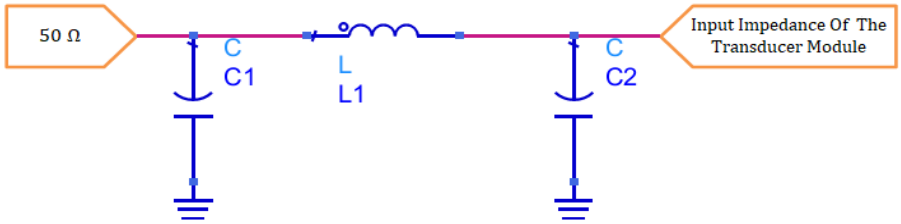

Figure 11. Pi matching network between 50 Ω antenna and RF-DC conversion module when the device is connected to its output.

Table 5. Lumped component values for each input impedance of the RF-DC converter module when devices are connected to its output.

Energized Device	Transducer Module input impedance with device connected (Ω)	The Q Value of Pi Impedance Matching Circuitry	The Value of Capacitor C_1 (pF)	The Value of Inductor L_1 (nH)	The Value of Capacitor C_2 (pF)
TMP20 Temperature Sensor	$48.8 - j205$	4.2	5.36	345.05	0.009
Light Emitting Diode	$51 - j200$	4.0	4.52	329.72	0.16
Panasonic VL2020 Battery	$56.1 - j193$	3.7	4.12	305.82	0.57

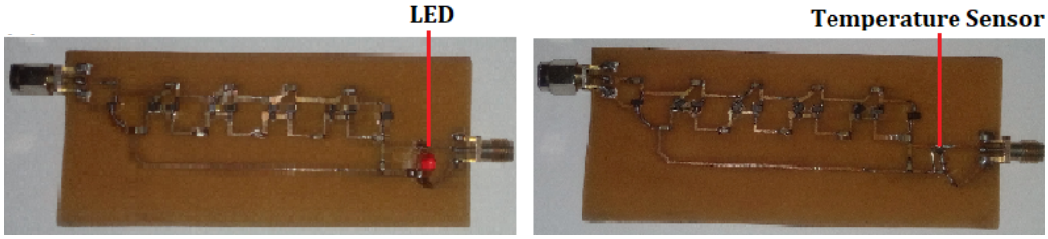

Figure 12. Transducer circuits with (a) LED and (b) temperature sensor connected to its output.

4. THE RF-DC CONVERSION MODULE

This section discusses the RF-DC conversion module at length under two main categories; i. Methodology of an RF-DC conversion module. ii. performance of the RF-DC conversion module.

4.1. Methodology of an RF-DC Conversion Module

The voltage multiplier circuitry is a conversion module that converts radio frequency power to direct current (DC) and sufficiently increases the output voltage for energizing low power devices. The Cockcroft-Walton (also called as a Villard) voltage multiplier and Dickson voltage multiplier are the main types of voltage multipliers that are employed in RF-DC conversion modules. There is no significant

difference between the output voltages of these two topologies [29]. The Cockcroft-Walton voltage multiplier topology was used to design the conversion circuitry. More rectifier stages increase the wastage of energy due to energy loss along the chain. Therefore, a 5-stage voltage multiplier circuit was designed and constructed for the RF energy harvesting system. The conversion circuit was tested with an impedance matching network through a waveform generator for various input power levels at 98 MHz. The circuit was measured 3 mV across the 100 kΩ for −45 dBm input power.

The RF-DC conversion module was designed by using HSMS-2850 Schottky detector diodes from HP/AVAGO. Due to the low series resistance and low forward voltage drop of these diodes, the energy loss through the doubler chain could be reduced. The low junction capacitance of this diode is faster as the voltage rises.

Each independent stage of the voltage multiplier circuitry with its dedicated voltage doubler circuit can be shown as a battery that has open circuit output voltage V_0 and internal resistance R_0 with a load resistance R_L. The output voltage V_{OUT} can be given by Equation (3) [30].

$$V_{OUT} = \frac{V_0}{R_0 + R_L} R_L \tag{3}$$

when n number of these circuits are linked together and connected to R_L, the output voltage across the load R_L can be given by Equation (4) [30].

$$V_{OUT} = \frac{nV_0}{nR_0 + R_L} R_L = V_0 \frac{1}{\frac{R_0}{R_L} + \frac{1}{n}} \tag{4}$$

According to Equation (4), the output voltage across the load can be increased by increasing the number of stages of the voltage multiplier circuitry.

4.2. Performance of the RF-DC Conversion Module

The implementation work was carried out through the 88 MHz to 108 MHz frequency range. The voltage across the 100 kΩ load was recorded for various input signal strength levels from −45 dBm to +5 dBm with an interval of 5 dBm through an arbitrary waveform generator. The Pi impedance matching network was connected for transmission of all the power into the voltage multiplier circuit that came from the signal generator.

As shown in Figure 13, the conversion circuitry was connected through SMA connectors to impedance matching circuitry.

To investigate the performance of the voltage multiplier circuits, the impedance matching network was connected to an input of the voltage multiplier, and testing was carried out at location 1. The output voltages after each doubler stage were recorded. The results are shown in Figure 13. Regular

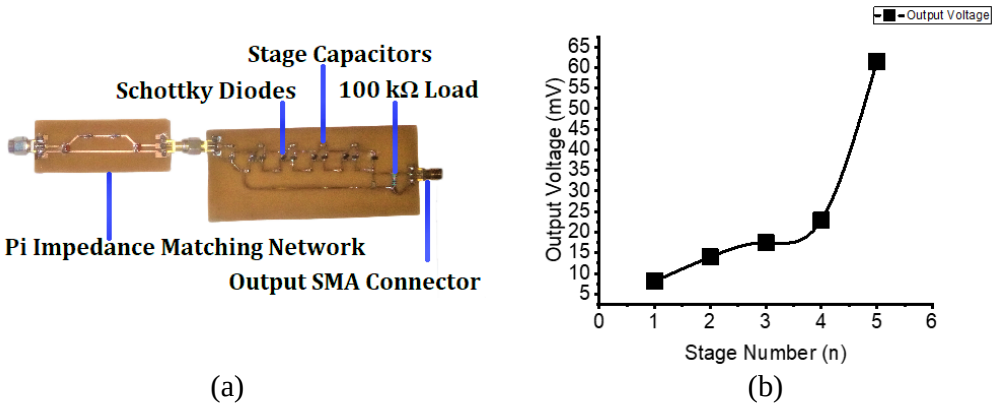

Figure 13. (a) Assembled circuit board of 5-stage voltage doubler connected to impedance matching network along with (b) the graph of output voltage versus the stage number.

voltage increase is shown in the first four multiplier stages. After four stages, the voltage begins to rapidly increase, and 61.5 mV is shown across the 100 kΩ at stage five. Afterward, a rapid increase in voltage can be observed, and outstretching the doubler chain will be affected to increase energy loss. Therefore, multiplier stages were bounded to five.

5. RESULTS OF RF POWER HARVESTING SYSTEM

An RF energy harvesting system was employed for energizing the TMP20 temperature sensor, Light-emitting diode, and Panasonic VL2020 rechargeable battery.

The TMP20 integrated circuit is an analog temperature sensor that can measure ambient temperature. It is a low-power device that has an operating voltage range of 1.8 V to 5.5 V with a 4 µA maximum supply current with ±2.5° accuracy [30].

The transfer function is shown in Equation (5), which can be used to measure environment temperature [31].

$$T = -1481.96 + \sqrt{2.1962 \times 10^2 + \frac{1.8639 - V_0}{3.88 \times 10^{-6}}} \tag{5}$$

The temperature sensor was activated in the laboratory by employing a power amplifier. The 2 W power amplifier was constructed and connected to the signal generator, and the amplifier was fed by a 98 MHz signal from the signal generator. The displacement between the antenna and harvesting system was preserved at 3 m.

The field test of the temperature sensor was carried out at ground level with a 500 m displacement from the FM radio channel transmission tower. The temperature that was read by the temperature sensor was compared with a thermometer reading and is presented in Table 6.

Table 6. Results of temperature sensor activation by RF energy harvesting system.

Test Environment	Input Voltage of Sensor (V)	Analog Output Voltage Through Sensor (°C)	Evaluated Through Sensor (°C)	Measured Temperature Through Thermometer (°C)
Field	4.21	1.476	33.35	33.0
Laboratory	4.00	1.548	27.23	28.2

The light-emitting diode was illuminated from location 2. As shown in Figure 14, the light-emitting diode turned on with a 1.75 V voltage drop across it.

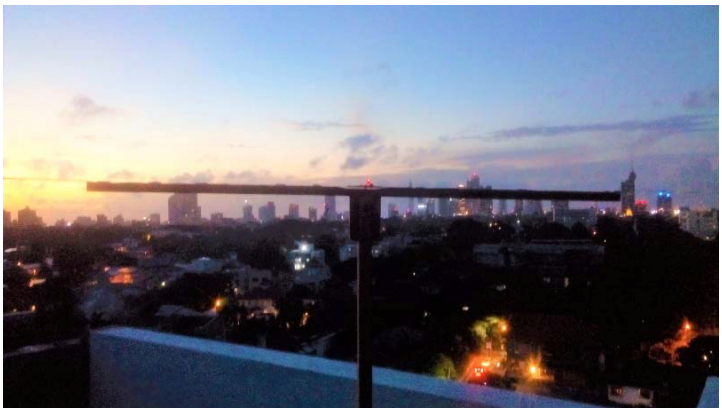

Figure 14. A picture of the illuminating light-emitting diode at location 2.

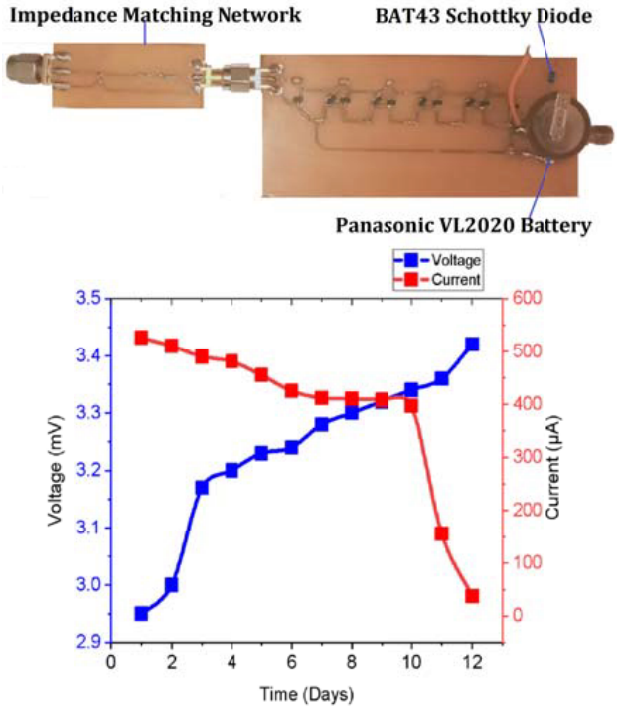

Figure 15. A photograph of assembled battery charger circuitry along with the charging voltage (V) versus time (in days) curve and charging current (μA) versus time (in days) curve of the battery.

In order to demonstrate the possibility of storing the harvested radio-frequency energy for later use, a Panasonic VL2020 rechargeable battery was used. This battery has a 20 mAh capacity and 3 V voltage. The diameter and thickness of the battery are 20 mm and 2 mm in order. It contains vanadium pentoxide lithium as a chemical compound.

As shown in Figure 15, a BAT43 Schottky diode was connected in series with the battery for the protection of the voltage multiplier circuitry by the reverse voltage of the battery. Specific features of this diode are high reverse breakdown voltage, very low current leaks when a reverse voltage is applied across it, and the low forward voltage drops across it.

The battery was fully discharged prior to connection. The battery charging process was carried out at location 2. The charging current curve and charging voltage curve of the battery are shown in Figure 15. The battery can be fully charged in 12 days.

6. CONCLUSION

A novel 88–108 MHz radio frequency band energy harvesting system was designed, optimized, implemented, and tested. A dynamic Pi impedance matching technique was discovered for radio-frequency harvesting systems. The impedance matching technique was theoretically described, and the simulation results agreed well with those of theory.

A copper plate dipole antenna was designed and constructed with 50 Ω impedance at 88–108 MHz range which is within the global frequency modulated radio band. The voltage doubler stages were preserved to 5 stages for injecting sufficient voltage for powering low power devices. A system was designed to collect radio-frequency energy for later uses, and it is capable of harvesting 2 mW RF energy at a distance of 760 m from a transmission tower. A TMP20 temperature sensor and a light-emitting diode were powered by the harvesting system.

The low Q value of the Pi impedance matching network is more suitable for radio-frequency harvesting systems due to their more negative reflection coefficient through the entire band. The 88–108 MHz radio frequency band is suitable for harvesting a significant amount of radio frequency

power at a significant displacement from the transmission tower.

It was shown that a Panasonic VL2020 rechargeable battery (20 mAh) could be fully charged over 12 days by the harvesting system. To gradually reduce this charging time, more power needs to be added to the energy storage system. Therefore, the proposed system will be improved as a multi-band RF harvesting system that can harvest both VHF and UHF band frequencies in the future.

ACKNOWLEDGMENT

The authors would like to thank the University of Sri Jayewardenepura (Grant No. ASP/01/RE/SCI/20-19/18) for the funding support.

REFERENCES

1. Geran, F., N. Mirzababaee, and S. Mohanna, "RF power harvester using a broadband monopole antenna and a quad-band rectifier," *International Journal of Industrial Electronics, Control and Optimization*, 2020.
2. Mouapi, A., N. Hakem, and N. Kandil, "Design of 900 MHz radio frequency energy harvesting circuit for the internet of things applications," *2020 IEEE International Conference on Environment and Electrical Engineering and 2020 IEEE Industrial and Commercial Power Systems Europe (EEEIC/I&CPS Europe)*, 1–6, IEEE, June 2020.
3. Md. Din, N., C. K. Chakrabarty, A. Bin Ismail, K. K. A. Devi, and W.-Y. Chen, "Design of RF energy harvesting system for energizing low power devices," *Progress In Electromagnetics Research*, Vol. 132, 49–69, 2012.
4. Moghaddam, N. A., A. Maleki, M. Shirichian, and N. S. Panah, "RF energy harvesting system and circuits for charging of wireless devices using spectrum sensing," *2017 24th IEEE International Conference on Electronics, Circuits and Systems (ICECS)*, 431–436, IEEE, December 2017.
5. Arrawatia, M., M. S. Baghini, and G. Kumar, "RF energy harvesting system from cell towers in 900 MHz band," *2011 National Conference on Communications (NCC)*, 1–5, IEEE, January 2011.
6. Gunathilaka, W. M. D. R., H. G. C. P. Dinesh, G. G. C. M. Gunasekara, K. M. M. W. N. B. Narampanawe, and J. V. Wijayakulasooriya, "Ambient radio frequency energy harvesting," *2012 IEEE 7th International Conference on Industrial and Information Systems (ICIIS)*, 1–5, IEEE, August 2012.
7. Arrawatia, M., M. S. Baghini, and G. Kumar, "Differential microstrip antenna for RF energy harvesting," *IEEE Transactions on Antennas and Propagation*, Vol. 63, No. 2, 1581–1588, 2015.
8. Colaiuda, D., I. Ulisse, and G. Ferri, "Rectifiers' design and optimization for a dual-channel RF energy harvester," *Journal of Low Power Electronics and Applications*, Vol. 10, No. 1, 11, 2020.
9. Farinholt, K. M., G. Park, and C. R. Farrar, "RF energy transmission for a low-power wireless impedance sensor node," *IEEE Sensors Journal*, Vol. 9, No. 7, 793–800, 2009.
10. Chang, Y., P. Zhang, and L. Wang, "Highly efficient differential rectenna for RF energy harvesting," *Microwave and Optical Technology Letters*, Vol. 61, No. 12, 2662–2668, 2019.
11. Chiam, T. M., L. C. Ong, M. F. Karim, and Y. X. Guo, "5.8 GHz circularly polarized rectennas using schottky diode and LTC5535 rectifier for RF energy harvesting," *2009 Asia Pacific Microwave Conference*, 32–35, IEEE, December 2009.
12. Pham, B. L. and A. V. Pham, "Triple bands antenna and high efficiency rectifier design for RF energy harvesting at 900, 1900 and 2400 MHz," *2013 IEEE MTT-S International Microwave Symposium Digest (MTT)*, 1–3, IEEE, June 2013.
13. Elsheakh, D., M. Farouk, H. Elsadek, and H. Ghali, "Quad-band rectenna for RF energy harvesting system," *Journal of Electromagnetic Analysis and Applications*, Vol. 12, No. 3, 57–70, 2020.
14. Kumar, H., M. Arrawatia, and G. Kumar, "Broadband planar log-periodic dipole array antenna based RF-energy harvesting system," *IETE Journal of Research*, Vol. 65, No. 1, 39–43, 2019.
15. Ungan, T. and L. M. Reindl, "Harvesting low ambient RF-sources for autonomous measurement systems," *2008 IEEE Instrumentation and Measurement Technology Conference*, 62–65, IEEE, May 2008.

16. Le, T., K. Mayaram, and T. Fiez, "Efficient far-field radio frequency energy harvesting for passively powered sensor networks," *IEEE Journal of Solid-State Circuits*, Vol. 43, No. 3, 1287–1302, 2008.
17. Jabbar, H., Y. S. Song, and T. T. Jeong, "RF energy harvesting system and circuits for charging of mobile devices," *IEEE Transactions on Consumer Electronics*, Vol. 56, No. 1, 247–253, 2010.
18. Scorcioni, S., L. Larcher, and A. Bertacchini, "Optimized CMOS RF-DC converters for remote wireless powering of RFID applications," *2012 IEEE International Conference on RFID (RFID)*, 47–53, IEEE, April 2012.
19. Gao, H., M. K. Matters-Kamrnerer, P. Harpe, D. Milosevic, U. Johannsen, A. van Roermund, and P. Baltus, "A 71 GHz RF energy harvesting tag with 8% efficiency for wireless temperature sensors in 65 nm CMOS," *2013 IEEE Radio Frequency Integrated Circuits Symposium (RFIC)*, 403–406, IEEE, June 2013.
20. Cepeda Rubio, M. F. J., G. D. Guerrero López, F. Valdés Perezgasga, F. Flores García, A. Vera Hernández, and L. Leija Salas, "Computer modeling for microwave ablation in breast cancer using a coaxial slot antenna," *International Journal of Thermophysics*, Vol. 36, Nos. 10–11, 2687–2704, 2015.
21. Gas, P. and J. Czosnowski, "Calculation of the coaxial-slot antenna characteristics used for the interstitial microwave hyperthermia treatment," *Przeglad Elektrotechniczny*, Vol. 90, No. 3, 176–178, 2014.
22. Gas, P., "Optimization of multi-slot coaxial antennas for microwave thermotherapy based on the S_{11}-parameter analysis," *Biocybernetics and Biomedical Engineering*, Vol. 37, No. 1, 78–93, 2017.
23. Bertram, J. M., D. Yang, M. C. Converse, J. G. Webster, and D. M. Mahvi, "Antenna design for microwave hepatic ablation using an axisymmetric electromagnetic model," *Biomedical Engineering Online*, Vol. 5, No. 1, 1–9, 2006.
24. Bird, T. S., "Definition and misuse of return loss [report of the transactions editor-in-chief]," *IEEE Antennas and Propagation Magazine*, Vol. 51, No. 1, 166–167, 2009.
25. Khalid, F., W. Saeed, N. Shoaib, M. U. Khan, and H. M. Cheema, "Quad-band 3D rectenna array for ambient RF energy harvesting," *International Journal of Antennas and Propagation, 2020*, 2020.
26. Park, J. K., Y. H. Cho, J. M. Kim, S. H. Kim, J. S. Yoo, W. Y. Lee, I. Y. Lee, J. S. Kim, and D. H. Kim, "FM radio chip antenna using magneto-dielectric," *2007 Asia-Pacific Microwave Conference*, 1–3, IEEE, December 2007.
27. Borja, C., J. Anguera, C. Puente, and J. Vergés, "How much can be reduced the internal FM antenna of mobiles phones?," *Proceedings of the Fourth European Conference on Antennas and Propagation*, 1–5, IEEE, April 2010.
28. Bowick, C., C. Ajluni, and J. Blyler, *RF Circuit Design*, Elsevier, Amsterdam, 2008.
29. Yan, H., J. M. Montero, A. Akhnoukh, L. C. De Vreede, and J. Burghartz, "An integration scheme for RF power harvesting," *Proc. STW Annual Workshop on Semiconductor Advances for Future Electronics and Sensors*, Vol. 2005, 64–66, November 2005.
30. Devi, K. K. A., N. M. Din, and C. K. Chakrabarthy, "Optimization of the voltage doubler stages in an RF-DC convertor module for energy harvesting," *Circuits and Systems*, Vol. 3, No. 3, Jul. 2012.
31. Ti.com. 2021. [online] Available at: https://www.ti.com/lit/ds/symlink/tmp20.pdf?ts=161210780-8539&ref_url=https%253A%252F%252Fwww.google.com%252F [Accessed 26 July 2020].